

Dark energy parameterizations and their effect on dark halos

Lamartine Liberato and Rogerio Rosenfeld

Instituto de Física Teórica- State University of São Paulo
Rua Pamplona 145, 01405-900, São Paulo, SP, Brazil.

E-mail: liberato@ift.unesp.br, rosenfel@ift.unesp.br

Abstract. There is a plethora of dark energy parameterizations that can fit current supernovae Ia data. However, this data is only sensitive to redshifts up to order one. In fact, many of these parameterizations break down at higher redshifts. In this paper we study the effect of dark energy models on the formation of dark halos. We select a couple of dark energy parameterizations which are sensible at high redshifts and compute their effect on the evolution of density perturbations in the linear and non-linear regimes. Using the Press-Schechter formalism we show that they produce distinguishable signatures in the number counts of dark halos. Therefore, future observations of galaxy clusters can provide complementary constraints on the behavior of dark energy.

Keywords: dark energy, dark halos, number counts

1. Introduction

There are strong and converging evidences suggesting that the universe is nearly flat and that the dominant component of the energy density today has an unknown nature. Analysis of the luminosity distance of high redshift Type Ia supernovae has led to the conclusion that the expansion of the universe is accelerating, with indications that this acceleration is recent [1, 2, 3, 4, 5] and are corroborated by cosmic microwave background radiation [6, 7] and large scale structure observations [8, 9].

This suggests that the dominant contribution to the present-day energy budget can be described by a fluid with equation of state $\omega < -1/3$, usually called “dark energy”. We do not know for sure what this dark energy really is and in our ignorance many parameterizations for the time or redshift dependence of the equation of state $\omega(z)$ have been introduced in order to observationally constrain its evolution.

Type Ia supernovae data are sensitive to $\omega(z)$ only for a small range of redshifts, typically up to $z = \mathcal{O}(1)$. This is the reason for the large allowed regions of parameters related to the variations of $\omega(z)$. In fact, the simplest possibility, a cosmological constant with $\omega(z) = -1$ still provides a good fit to the data. Therefore, it would be highly desirable to have another observable, sensitive to higher redshifts, that could break the degeneracy among the several different proposed parameterizations.

Dark energy has a dramatic effect on the dynamics of the universe, altering the way in which cosmological structures grow [10]. This offers the possibility that observations of structure formation may provide a sensitive probe of dark energy properties that is complementary to information derived from supernovae data.

The build-up of structure in universes with dark energy is subject to significant ongoing study [11, 12, 13, 14, 15, 16, 17, 18, 19, 20, 21], particularly through the spherical collapse model [22] in association with the Press-Schechter formalism for the mass function [23]. In this paper we use these techniques to investigate cosmologies in which the dark energy component remains homogeneous on the scales of the structures being modelled and their consequences to structure formation, in special to the cluster number counts. In particular, we show that cluster number counts can be sensitive to the different parameterizations of the dark energy equation of state.

This paper is organized as follows. In section 2 we show the parameterizations we will be using to illustrate our results. In section 3 we study how the linear growth of perturbations is affected by these models of dark energy. Section 4 is devoted to the non-linear growth of perturbations in the spherical collapse model and the computation of the threshold density contrast for collapse in the different models studied. In section 5 we present our results for the number counts of dark halos in different mass bins and also an integrated count in the different models studied. Finally, our conclusions are presented in section 6.

2. Parameterizations for the dark energy equation-of-state

The expansion history of the universe is determined by the Hubble parameter, $H(t) = \dot{a}/a$, where $a(t)$ is the scale factor ($a(t_0) \equiv a_0 = 1$ today). We assume that the dark energy has an equation of state relating its pressure p_{DE} and density ρ_{DE} at a particular instant determined by $a(t)$ given by $p_{DE} = \omega(a)\rho_{DE}$ and that matter is pressureless, $p_M = 0$. For general $\omega(a)$, the expansion rate of the universe is governed by the Friedman equation

$$\frac{H^2(a)}{H_0^2} = \Omega_M^{(0)} a^{-3} + \Omega_K a^{-2} + \Omega_{DE}^{(0)} e^{f(a)}, \quad (1)$$

where $\Omega_M^{(0)}$, Ω_K and $\Omega_{DE}^{(0)}$ are the current density parameters due to non-relativistic matter (baryonic and non-baryonic), curvature and dark energy. In the following we assume a flat universe, $\Omega_K \equiv (1 - \Omega_M - \Omega_{DE}) = 0$. H_0 is the Hubble constant and the function $f(a)$ is determined by the dark energy equation of state:

$$f(a) = 3 \int_a^1 [1 + \omega(a')] d \ln a'. \quad (2)$$

The matter density $\Omega_M(a)$ and dark energy density $\Omega_{DE}(a)$ are functions of a :

$$\Omega_M(a) = \Omega_M^{(0)} a^{-3} \frac{H_0^2}{H^2(a)}, \quad (3)$$

and

$$\Omega_{DE}(a) = \Omega_{DE}^{(0)} e^{f(a)} \frac{H_0^2}{H^2(a)}. \quad (4)$$

Throughout this paper we will adopt $\Omega_M^{(0)} = 0.25$, $\Omega_{DE}^{(0)} = 0.75$, $H_0 = 72 \text{ km s}^{-1} \text{ Mpc}^{-1}$ [7] and use either the scale parameter a or the corresponding redshift $z = (1 - a)/a$ to describe the evolution of the different parameters.

Recently discovered Type Ia supernovae (SNeIa) [4, 5] provide conclusive evidence of the decelerating universe in the past ($z > 0.5$) evolving into the present day accelerating universe. Thus the existence of dark energy, which accelerates the cosmic expansion, has been firmly established and the magnitude of its energy density today has been accurately measured. The goal is now to determine the behavior of the dark energy density and its equation of state at different cosmic epochs. The simplest and most natural candidate for dark energy is the cosmological constant Λ with a constant energy density Ω_Λ and a fixed equation of state parameter $\omega = -1$. It still provides a good fit to SNeIa data.

The exact functional form of the equation of state $\omega(z)$ should follow from a fundamental theory for the dark energy. The best studied case is the so-called quintessence models, where dark energy results from a scalar field rolling down a potential. In this class of models, the equation of state is strictly in the region $-1 < \omega < 1$. However, more complicated models with multiple scalar fields or non-canonical kinetic energy can have $\omega < -1$.

In the absence of a physically well-motivated fundamental theory for dark energy, it has become common practice to adopt parametric forms of $\omega(z)$ and to use SNeIa data to find the allowed regions in the parameter space for different parameterizations [15, 24, 25, 26, 27, 28].

Many parameterizations were proposed to fit the observations and some of them are shown in Table 1.

Table 1. Different parameterizations for dark energy (some of these models are from [28])

| Model | $H^2(z)$ or $\omega(z)$ | Parameters |
|-----------|--|--|
| Ia | $\omega(z) = \omega_0 + \omega_1 \frac{z}{(1+z)^2} = \omega_0 + \omega_1(1-a)a$ | $\omega_0 = -1.3$ $\omega_1 = 4$ |
| Ib | $\omega(z) = \omega_0 + \omega_1 \frac{z}{(1+z)^2} = \omega_0 + \omega_1(1-a)a$ | $\omega_0 = -1.3$ $\omega_1 = -2$ |
| II | $\omega(z) = \omega_0 + \omega_1 \frac{z}{(1+z)^{1.8}} = \omega_0 + \omega_1(1-a)a^{0.8}$ | $\omega_0 = -1.3$ $\omega_1 = 4$ |
| III | $H^2(z) = H_0^2 [\Omega_M^{(0)}(1+z)^3 + \Omega_{DE}^{(0)} + a_1(1+z)^3[\cos(a_2 z + a_3 \pi) - \cos(a_3 \pi)]]$ | $a_1 = 0.13$ $a_2 = 6.83$ $a_3 = 4.57$ |
| IV | $H^2(z) = H_0^2 \{ \Omega_M^{(0)}(1+z)^3 + a_1(1+z) + a_2(1+z)^2 + (\Omega_{DE}^{(0)} - a_1 - a_2) \}$ | $a_1 = -4.16$ $a_2 = 1.67$ |
| V | $H^2(z) = H_0^2 [\Omega_M^{(0)}(1+z)^3 - \sqrt{a_1 + a_2(1+z)^3} (\Omega_{DE}^{(0)} + \sqrt{a_1 + a_2})]$ | $a_1 = 29.08$ $a_2 = -0.097$ |
| VI | $\omega(z) = \frac{\omega_0}{1+b \ln(1+z)}$ | $\omega_0 = -1$ $b = 0.25$ |
| VII | $\omega(z) = \omega_0 + \omega_1 z = \omega_0 + \omega_1 \frac{1-a}{a}$ | $\omega_0 = -1.4$ $\omega_1 = 1.67$ |
| VIII | $\omega(z) = \omega_0 + \omega_1 \frac{z}{1+z} = \omega_0 + \omega_1(1-a)$ | $\omega_0 = -1.4$ $\omega_1 = 1.67$ |
| Λ | $\omega = -1$ or $H^2(z) = H_0^2 [\Omega_M^{(0)}(1+z)^3 + \Omega_{DE}^{(0)}]$ | - |

The parameterizations or models shown in Table 1 are obtained from several sources. Models Ia and Ib are the same parameterization with the same central value of ω_0 but with values for ω_1 at the extrema of the range allowed by SNLS and WMAP [25, 31]. Model II is a slight modification of model I. Models III, IV and V are an oscillating, a quadratic polynomial and a brane-motivated ansatze for $H(z)$, respectively and we used the central values of the parameters [28]. Model VI was proposed by Wetterich [32] and its best fit parameters are taken from [18]. The parameterizations VII [24, 27] and VIII [15, 26] are first order Taylor expansions around $z = 0$ and around $a = 1$, respectively. In figure 1 we show the behavior of the dark energy densities resulting from these parameterizations up to $z = 5$ and we see that most of them

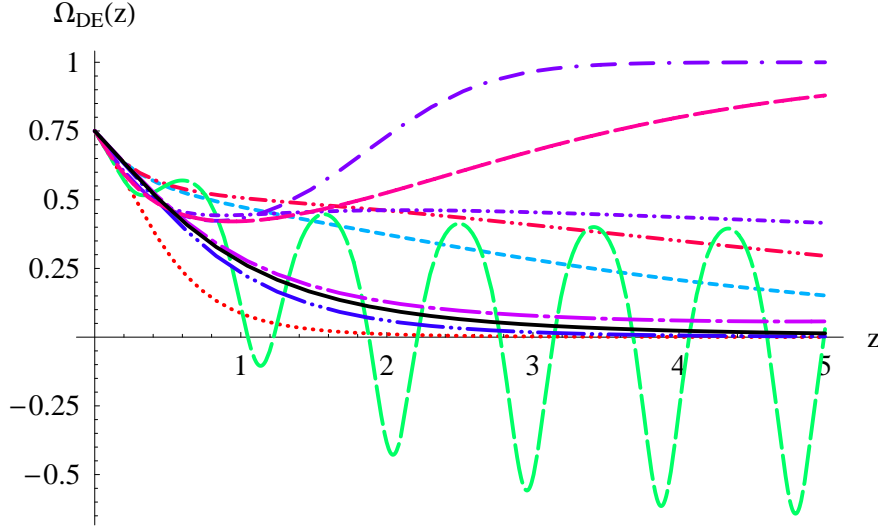


Figure 1. Evolution of the dark energy Ω_{DE} with redshift for parameterizations of Table 1. The lines are as follows: Λ CDM (solid), Ia (short dashed), Ib (dotted), II (double dot dashed), III (long dashed), IV (dot short dashed), V (dot long dashed), VI (double dot long dashed), VII (double dashed dotted), VIII (triple dot dashed).

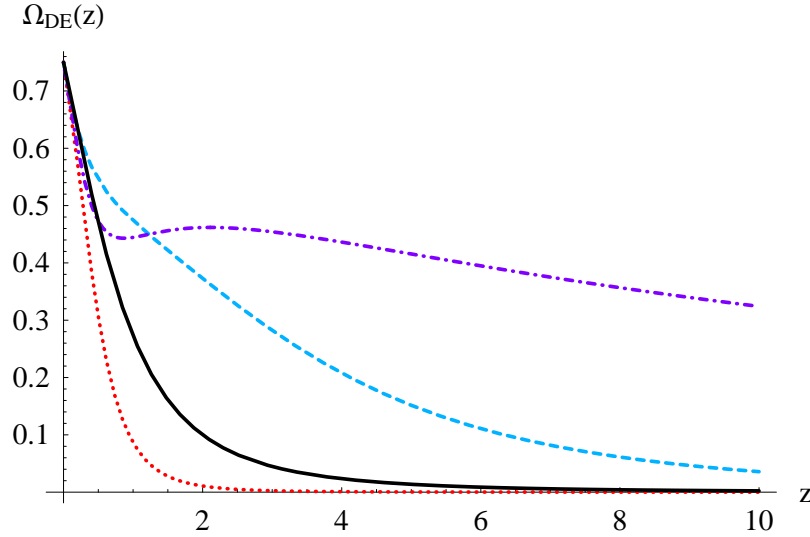


Figure 2. Evolution of the dark energy Ω_{DE} with redshift for selected models of Table 1. The lines are as follows: Λ CDM (solid), Ia (short dashed), Ib (dotted) and IV (dot short dashed).

present problems such as a too large dark energy component for redshifts higher than $z = 1$.

For our study we select only a couple of models with decreasing contribution of $\Omega_{DE}(z)$ in the past. In order to contrast with the Λ CDM model, we choose models with energy densities both above and below the one given by a cosmological constant. These are models Ia, Ib and IV, whose energy densities and equations of state are depicted in

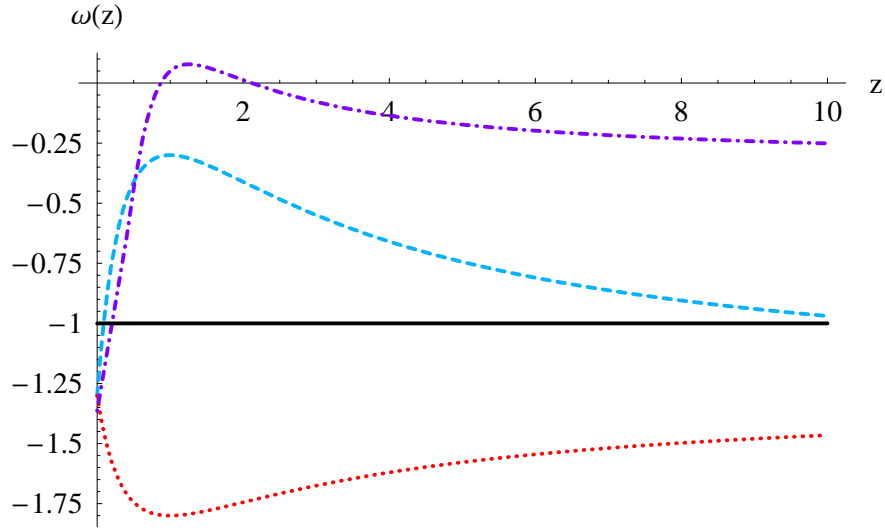


Figure 3. Equation of state evolution $\omega(z)$ with redshift for selected models of Table 1. Lines are the same as in figure 2.

figure 2 and figure 3.

In the next sections we investigate the consequences of these different models to cosmological parameters that are relevant for large scale structure formation in the universe.

3. Linear Perturbation Theory

We assume that the dark energy component is smooth on scales smaller than the horizon [34]. In this case we only need to consider perturbations to the non-relativistic matter component. Dark energy only alters the background evolution and the equation of perturbed density contrast (for perturbations larger than the Jeans length) is [38]

$$\ddot{\delta} + 2H(t)\dot{\delta} - \frac{3}{2}H(t)^2\Omega_M(t)\delta = 0, \quad (5)$$

where δ is the fractional matter density perturbation.

The growth function is defined as the ratio of the perturbation amplitude at some scale factor relative to some fixed scale factor, $D = \delta(a)/\delta(a_0)$, and its evolution equation can be written as

$$D'' + \frac{3}{2} \left[1 - \frac{\omega(a)}{1 + X(a)} \right] \frac{D'}{a} - \frac{3}{2} \frac{X(a)}{1 + X(a)} \frac{D}{a^2} = 0, \quad (6)$$

where the prime denotes derivative with respect to the scale factor a and $X(a)$ is the ratio of the matter density to the dark energy density:

$$X(a) = \frac{\Omega_M^{(0)}}{1 - \Omega_M^{(0)}} e^{-3 \int_a^1 d \ln a' \omega(a')} . \quad (7)$$

For large X one recovers the matter dominated behavior $D \sim a$. The ratio of the matter density to the dark energy density $X(z)$ can be seen in figure 4. Notice that for all models except model IV the dark energy contribution decreases rapidly with redshift. In model IV the dark energy density decreases slowly but for redshifts larger than 0.5 this parameterization does not accelerate the universe.

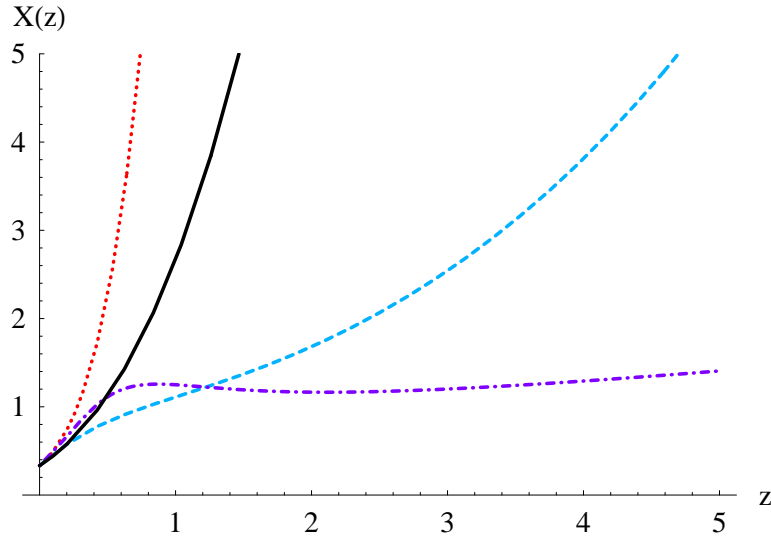


Figure 4. Behavior of the X with redshift for dark energy scenarios considered. Lines are the same as in figure 2.

In figure 5 we show the evolution of the growth function $D(z)$ for the selected dark energy models and for pure dark matter case. Notice that, as expected, larger perturbations in the past are needed to arise at the same amplitude today for models where dark energy is more important since negative pressure tends to inhibit the growth of perturbations.

4. Non-Linear Evolution of Perturbations

In order to describe the non-linear evolution of the density perturbations we adopt the spherical collapse model [22] where the radius $R(t)$ of a spherical homogeneous overdensity region obeys the curvature-independent Raychaudhuri equation:

$$\ddot{R} = -\frac{3}{2}\Omega_{DE}^{(0)}(w(a) + 1/3)e^{f(a)}R - \frac{1}{2}\Omega_M^{(0)}(1 + \Delta_i)\frac{1}{R^2}, \quad (8)$$

where time is measured in units of $1/H_0$ and Δ_i is the initial overdensity in the sphere. We numerically solved this equation for an initial time t_i where $a(t_i) = 10^{-5}$, with initial conditions chosen so that the sphere is initially in the Hubble flow, $R(t_i) = a(t_i)$, $\dot{R}(t_i) = \dot{a}(t_i)$. We find the values of Δ_i such that the collapse occurs today. The linear evolution of $\delta_i = \Delta_i$ until today results in the critical linear density contrast parameter δ_c which is important in the Press-Schechter [23] formalism discussed below. In figure 6

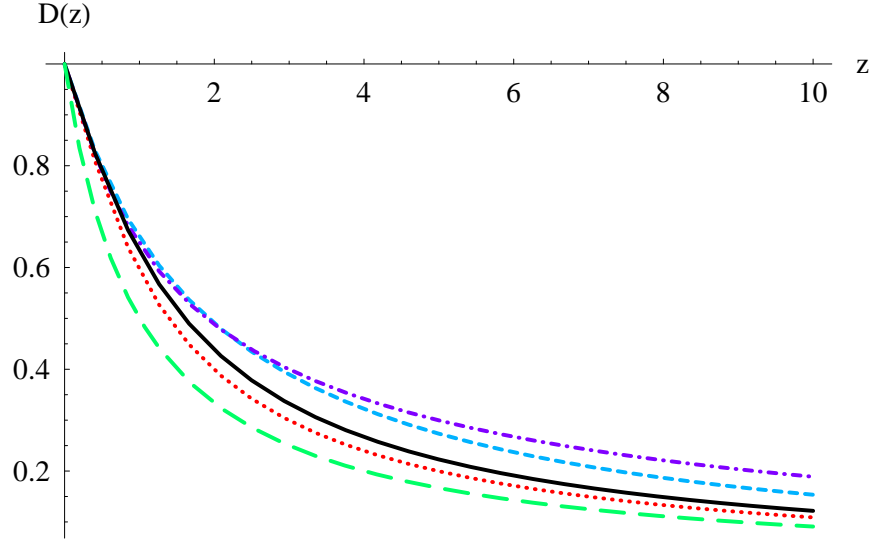


Figure 5. Evolution of the growth factor $D(z)$ with redshift for selected dark energy models (lines are the same as in figure (2)) and for pure dark matter case (in which case $D(z) = a(z) = \frac{1}{1+z}$) (long dashed line).

we show an example in the Λ CDM model of the linear and non-linear evolution for an initial overdensity of $\Delta_i = 10^{-4.446}$, chosen so that the collapse occurs today.

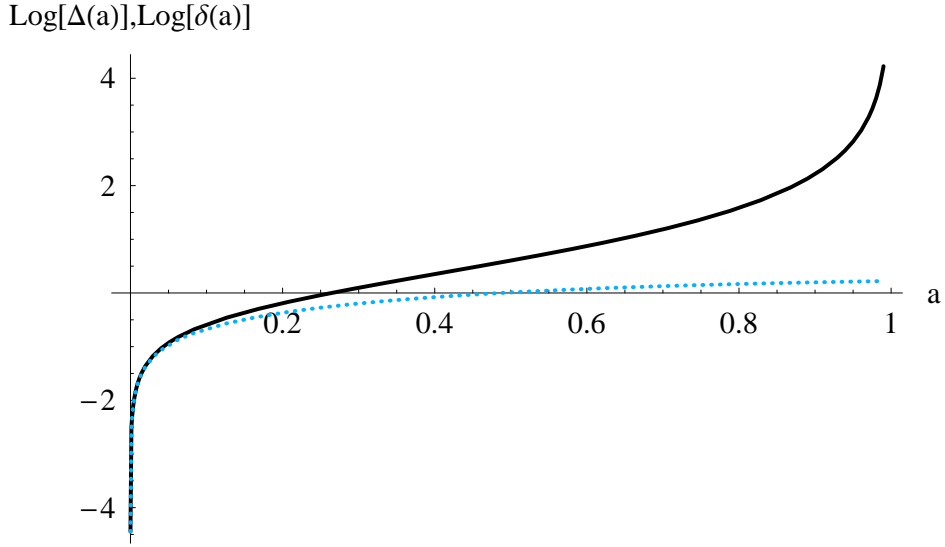


Figure 6. Evolution of the linear (dotted line) and non-linear (solid line) density contrasts in Λ CDM for an initial value chosen so that the collapse occurs today.

In an Einstein-de Sitter universe, an exact value of $\delta_c = 1.686$ is obtained [22] and we verified that this value is fairly independent of the background cosmology [16].

We have also computed the values of $\delta_c(z)$ for different collapse redshifts. Our results, shown in figure 7, find no large numerical differences among the models, in

agreement with [10, 37]. We use these values of $\delta_c(z)$ to compute the halo abundances in the next section.

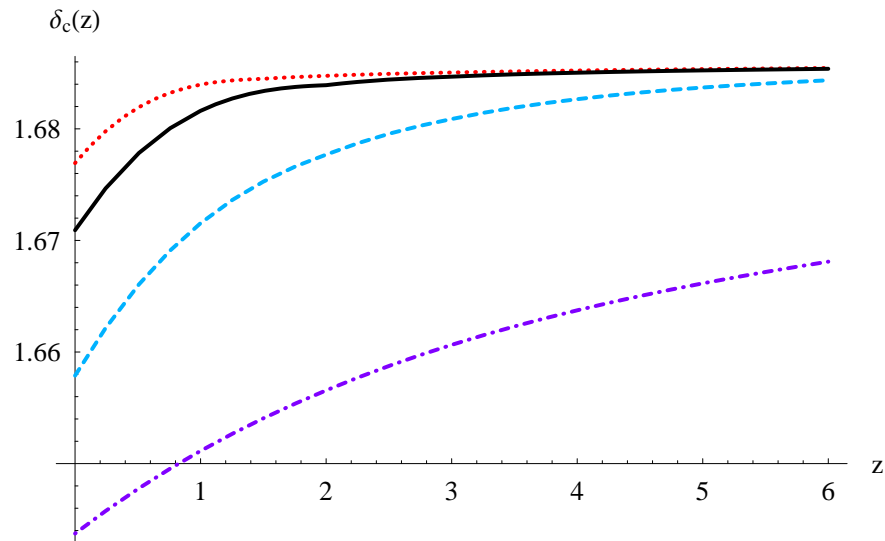


Figure 7. Threshold overdensity for different redshifts of collapse for the models considered. Lines are the same as in figure 2.

5. Mass Function and Cluster Number Counts

The most reliable method to study the cluster abundance in the universe is through numerical simulations. However, there is an analytical approximation, the Press-Schechter formalism [23], that has been shown to fairly reproduce the results of N-body simulations [35]. There are more recent and better approximations with extra free parameters [36] but as an initial step we will use the well-known Press-Schechter approach.

The basic premisses of the Press-Schechter formalism is to assume that the fraction of mass in the universe contained in gravitationally bound systems with masses greater than M is given by the fraction of space where the linearly evolved density contrast exceeds a threshold δ_c , defined in the previous section, and that the density contrast is normally distributed with zero mean and variance $\sigma^2(M)$, the root-mean-squared value of the density contrast δ at scales containing a mass M . Therefore, it is assumed that for a massive sphere to undergo gravitational collapse at a redshift z its linear overdensity should exceed a threshold $\delta_c(z)$. Notice that only linear quantities are used in this formalism.

These assumptions lead to the well-known analytical formula for the comoving number density of collapsed halos of mass in the range M and $M + dM$ at a given

redshift z :

$$\frac{dn}{dM} = -\sqrt{\frac{2}{\pi}} \frac{\rho_{\text{m}0}}{M} \frac{\delta_c(z)}{\sigma(M, z)} \frac{d \ln \sigma(M, z)}{dM} \exp \left[-\frac{\delta_c^2(z)}{2\sigma^2(M, z)} \right], \quad (9)$$

where $\rho_{\text{m}0}$ is the present matter mean density of the universe and $\delta_c(z)$ is the linearly extrapolated density threshold above which structures collapse, *i.e.*, $\delta_c(z) = \delta(z = z_{\text{col}})$.

The quantity

$$\sigma(M, z) = D(z)\sigma_M \quad (10)$$

is the linear theory *rms* density fluctuation in spheres of comoving radius R containing the mass M . The smoothing scale R is often specified by the mass within the volume defined by the window function at the present time, see *e.g.* [39]. In our analysis we use the fit given by [12]

$$\sigma_M = \sigma_8 \left(\frac{M}{M_8} \right)^{-\gamma(M)/3}, \quad (11)$$

where $M_8 = 6 \times 10^{14} \Omega_M^{(0)} h^{-1} M_\odot$ is the mass inside a sphere of radius $R_8 = 8h^{-1}\text{Mpc}$, and σ_8 is the variance of the over-density field smoothed on a scale of size R_8 . The index γ is a function of the mass scale and the shape parameter, $\Gamma = \Omega_M^{(0)} h e^{-\Omega_b - \Omega_b/\Omega_M^{(0)}}$ (Ω_b is the baryonic density parameter), of the matter power spectrum [12]

$$\gamma(M) = (0.3\Gamma + 0.2) \left[2.92 + \frac{1}{3} \log \left(\frac{M}{M_8} \right) \right]. \quad (12)$$

Denoting $\tilde{\gamma}(M) = \frac{d \ln \sigma(M, z)}{dM}$ (notice that it is z independent),

$$\tilde{\gamma}(M) = (0.3\Gamma + 0.2) \left[2.92 + \frac{2}{3} \log \left(\frac{M}{M_8} \right) \right], \quad (13)$$

we can rewrite (9) as

$$\frac{dn}{dM} = -\sqrt{\frac{2}{\pi}} \frac{\rho_{\text{m}0}}{M} \frac{\delta_c(z)}{\sigma(M, z)} \tilde{\gamma}(M) \exp \left[-\frac{\delta_c(z)^2}{2\sigma^2(M, z)} \right]. \quad (14)$$

In our study we use $\Gamma = 0.144$ [7]. For a fixed σ_8 (power spectrum normalization) the predicted number density of dark matter halos given by the above formula is uniquely affected by the dark energy models through the ratio $\delta_c(z)/D(z)$. In order to compare the different models, we will normalize to mass function to the same value today, that is, we will require

$$\sigma_{8,M} = \frac{\delta_{c,M}(z=0)}{\delta_{c,\Lambda}(z=0)} \sigma_{8,\Lambda}, \quad (15)$$

where the label M indicates a given model and we use $\sigma_{8,\Lambda} = 0.76$ [7]. We show in figure 8 the resulting mass functions for the different models.

The effect of dark energy on the number of dark matter halos is studied by computing two quantities. The first is the all sky number of halos per unit of redshift, in a given mass bin

$$\mathcal{N}^{\text{bin}} \equiv \frac{dN}{dz} = \int_{4\pi} d\Omega \int_{M_{\text{inf}}}^{M_{\text{sup}}} \frac{dn}{dM} \frac{dV}{dz d\Omega} dM, \quad (16)$$

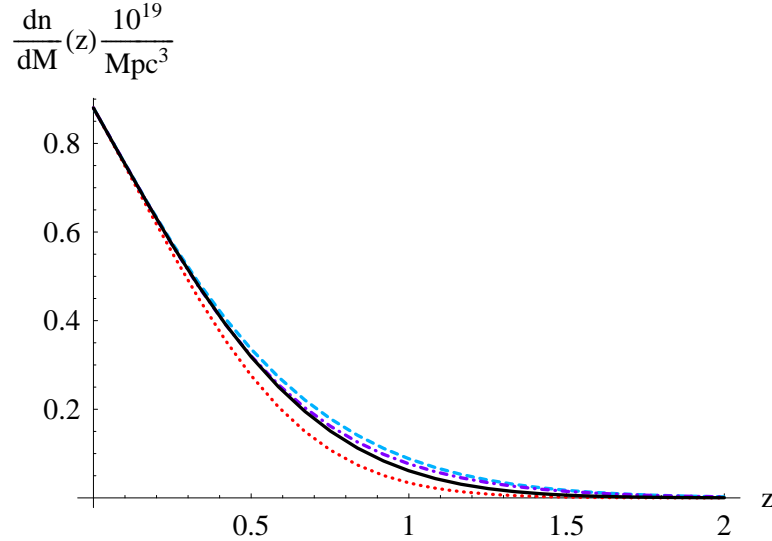


Figure 8. Press-Schechter mass functions for the different models with the σ_8 normalization. Lines are the same as in figure 2.

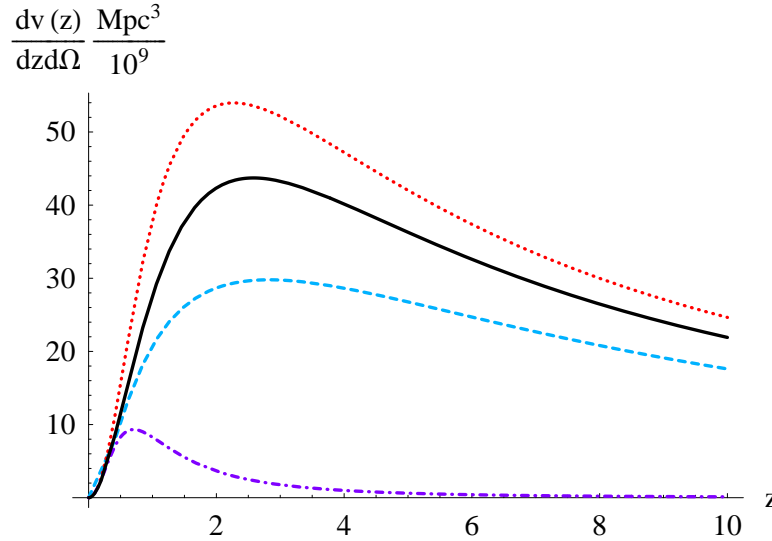


Figure 9. Evolution of the comoving volume element with redshift for the four dark energy scenarios considered in this paper. Lines are the same as in figure 2.

where the comoving volume element is given by

$$dV/dz d\Omega = r^2(z)/H(z), \quad (17)$$

where $r(z) = \int_0^z H^{-1}(x)dx$ is the comoving distance. The redshift evolution of the comoving volume element $dV/dz d\Omega$ for different models of dark energy is shown in figure 9. Note that the comoving volume element does not depend on the growth factor of the perturbation $D(z)$, but only on the cosmological background. The comoving volume element is larger for more negative equation-of-state, since this implies larger acceleration, see figure 3.

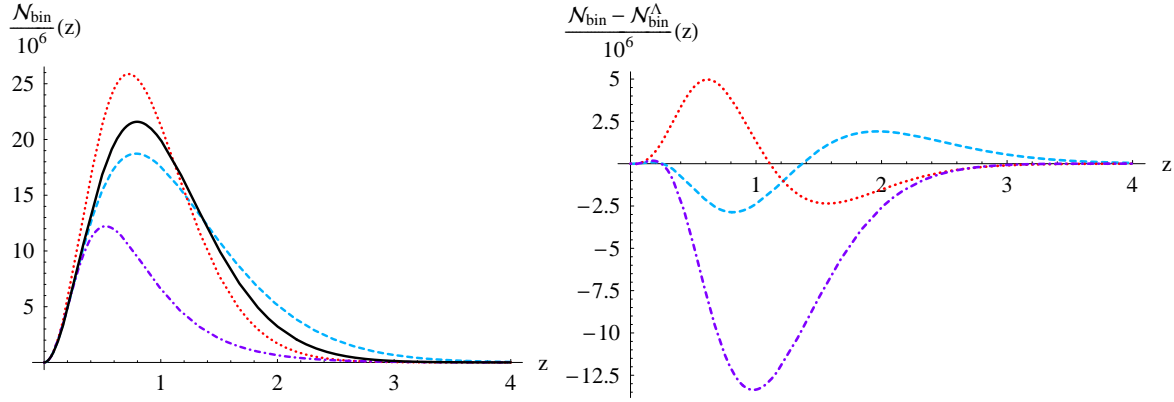


Figure 10. Evolution of number counts in mass bins with redshift for objects with mass within the range $10^{13} < M/(h^{-1} M_\odot) < 10^{14}$. Notice the normalization factor of $\frac{N}{10^6}$. Lines are the same as in figure 2.

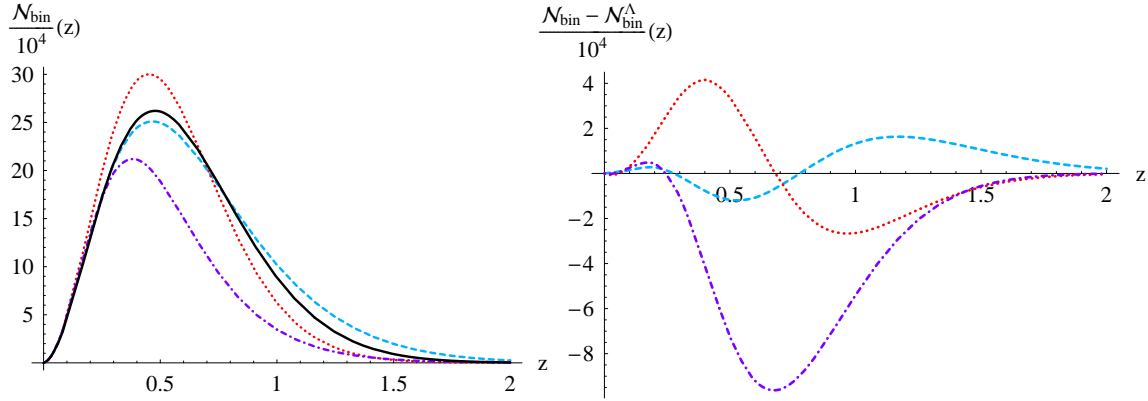


Figure 11. Evolution of number counts in mass bins with redshift for objects with mass within the range $10^{14} < M/(h^{-1} M_\odot) < 10^{15}$. Notice the normalization factor of $\frac{N}{10^4}$. Lines are the same as in figure 2.

The second quantity we compute is the all sky integrated number counts above a given mass threshold, M_{inf} , and up to redshift z [20]:

$$N(z, M > M_{\text{inf}}) = \int_{4\pi} d\Omega \int_{M_{\text{inf}}}^{\infty} \int_0^z \frac{dn}{dM} \frac{dV}{dz' d\Omega} dM dz'. \quad (18)$$

Our knowledge of both these quantities for galaxy clusters will improve enormously with upcoming cluster surveys operating at different wavebands.

The modifications caused by a dark energy component on the number of dark matter halos are tested and confronted with a cosmological constant Λ CDM model. We examine the effects of the different equations of state on the number of dark matter halos in mass bins $[M_{\text{inf}}, M_{\text{sup}}]$ illustrating different classes of cosmological structures, namely $[10^{13}, 10^{14}]$, $[10^{14}, 10^{15}]$ and $[10^{15}, 10^{16}]$ in units of $h^{-1} M_\odot$.

The number counts in mass bins, $\mathcal{N}^{\text{bin}} = dN/dz$, obtained from (16), are shown in figures 10, 11 and 12. In each of these figures we plot in the left panel the actual

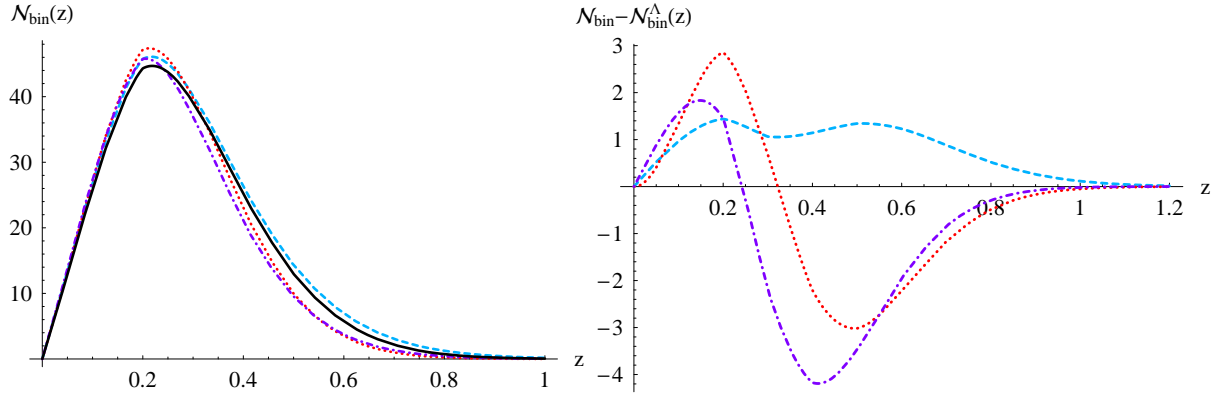


Figure 12. Same as figure 11 for objects with mass within the range $10^{15} < M/(h^{-1} M_{\odot}) < 10^{16}$. Note that here $\frac{N}{10}$ and z range different from figure 11. Lines are the same as in figure 2.

number counts and in the right panel we show the difference with the fiducial Λ CDM model. Notice that the more massive structures are less abundant and form at later times, as it should be in the hierarchical model of structure formation. Also there is a slight difference of the peak redshift for structure formation in the different dark energy models considered.

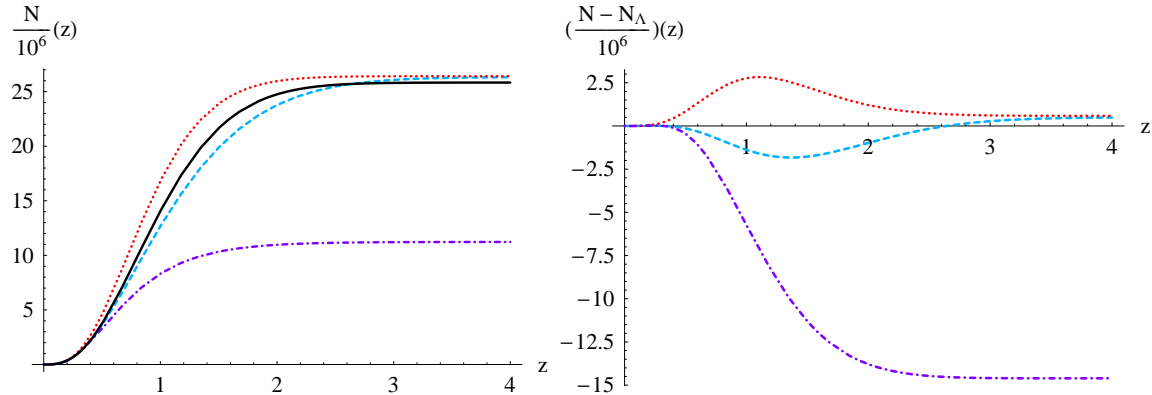


Figure 13. Evolution of the integrated number counts up to redshift z for objects with mass above $10^{13} h^{-1} M_{\odot}$. Lines are the same as in figure 2.

The difference among the models results from a competition between the different volume elements and the different growth functions. At redshifts below one the comoving volume element has the most important role in the integral of Eq. (16). Above this redshift the comoving volume element does not vary significantly and the growth function becomes the dominant source for the number counts.

An important observable quantity is the integrated number of collapsed structures above a given mass, equation (18). We present results for the integrated number counts of structures with masses above $10^{13} h^{-1} M_{\odot}$, $10^{14} h^{-1} M_{\odot}$, and $10^{15} h^{-1} M_{\odot}$. These are displayed in the figures 13, 14 and 15, together with the difference with

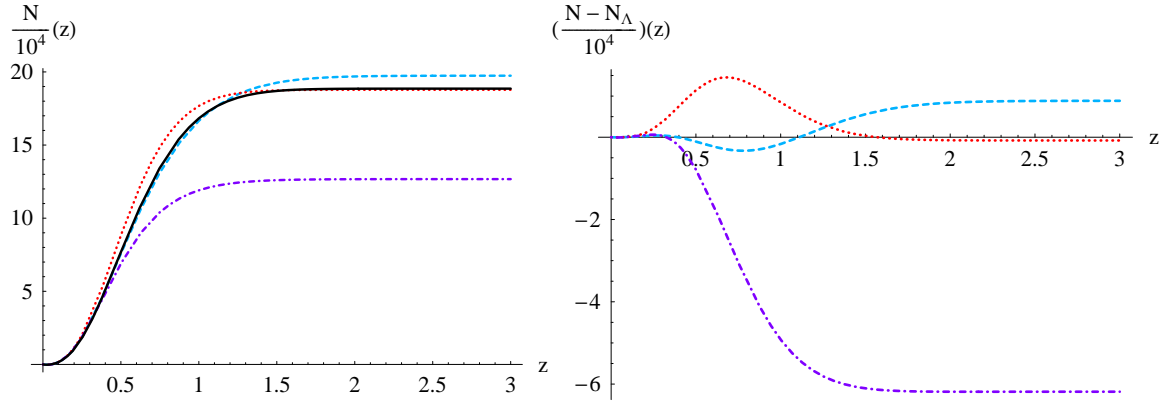


Figure 14. Evolution of the integrated number counts up to redshift z for objects with mass above $10^{14}h^{-1}M_{\odot}$. Lines are the same as in figure 2.

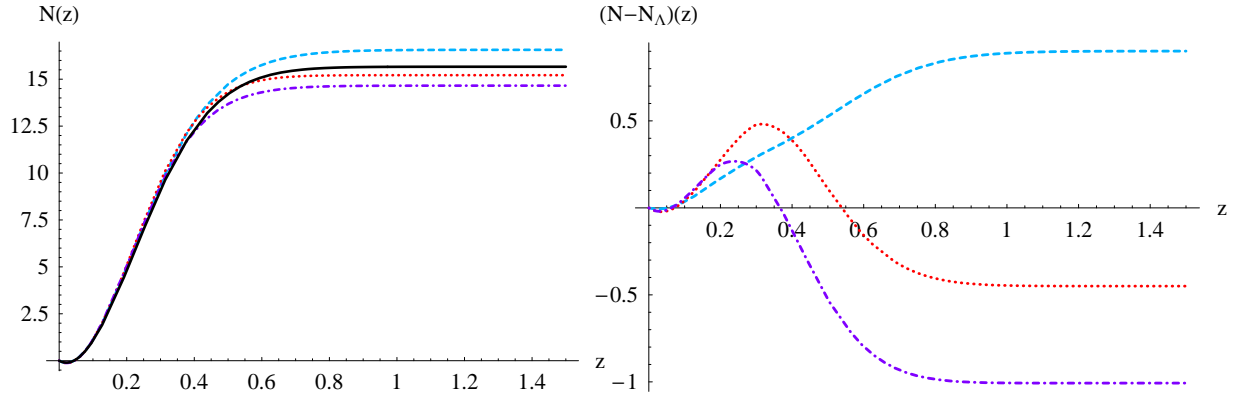


Figure 15. Evolution of the integrated number counts up to redshift z for objects with mass above $10^{15}h^{-1}M_{\odot}$. Lines are the same as in figure 2.

respect to the fiducial Λ CDM model. We cut-off the integration in equation (18) at $M_{\text{sup}} = 10^{18}h^{-1}M_{\odot}$. Notice that the integrated number has a plateau that reflects the epoch of structure formation for a given mass. In other words, there is no formation of structures with mass above $10^{13}h^{-1}M_{\odot}$, $10^{14}h^{-1}M_{\odot}$, and $10^{15}h^{-1}M_{\odot}$ for redshifts roughly above $z = 2$, 1 and 0.6 , respectively.

We notice that observations with accuracy of the order of 10%, either in binned or the integrated number counts, will be able to distinguish among the different models, providing important information on the nature of dark energy.

6. Conclusions

We know that universe is currently accelerating and several different mechanisms have been proposed to explain the data. In the absence of a definitive model, an approach widely used in the literature is to assume a given parameterization of the dark

energy equation of state. SNeIa data provides constraints in these parameterizations but are sensitive to redshifts up to $\mathcal{O}(1)$.

On the other hand, dark energy also influences the way in which the large scale cosmological structures form. In particular, number counts of collapsed structures is an important tool to probe dark energy models. Since structure formation occurs at redshifts higher than those probed by SNeIa, number counts can provide useful complementary information in order to constraint the parameters of the different proposed parameterizations of the dark energy equation of state.

In this paper we showed the impact of the different parameterizations and values for the parameters on several factors affecting large scale structure formation. We chose to exemplify our analysis by comparing a standard Λ CDM model with 2 parameterizations, one of them with two set of parameters currently allowed by data.

We use the spherical collapse model in conjunction with the Press-Schechter mass function to investigate the effect of dark energy on the linear and non-linear growth of density perturbations and on the number counts of collapsed structures in different mass and redshift ranges. The dominant effect on number counts seem to arise from the mass function, which is more important than the comoving volume factor. The corrections arising from the merging of clusters were shown to be small [14] and hence were not considered in this work.

Our results show that number counts can be useful in constraining dark energy models. Besides showing that the unintegrated and integrated number counts by themselves are powerful measurements, the redshift of maximum structure formation could also be used to differentiate the models. Observations with accuracy of the order of 10% can be used to distinguish among the different models, providing important information on the nature of dark energy.

On the observational side, there are new experiments planned to start taking data on the abundance of clusters in the near future. In particular, the South Pole Telescope survey, based on the detection of the Sunyaev-Zeldovich effect arising from inverse Compton scattering of background photons off the hot intra-cluster gas, is expected to find a large number of clusters and will be able to determine the number counts to a high accuracy [47]. Hopefully these future observations will be able to discriminate among different parameterizations of dark energy currently proposed.

Acknowledgements

We thank Reuven Opher and Ioav Waga for a careful reading of the manuscript and for providing useful suggestions and criticisms. The work of L.L. was supported by CAPES and the work of R.R. was partially supported by CNPq.

References

- [1] A. G. Riess *et al.* [Supernova Search Team Collaboration], Astron. J. **116**, 1009 (1998) [arXiv:astro-ph/9805201].

- [2] S. Perlmutter *et al.* [Supernova Cosmology Project Collaboration], *Astrophys. J.* **517**, 565 (1999) [arXiv:astro-ph/9812133].
- [3] R. A. Knop *et al.* [The Supernova Cosmology Project Collaboration], *Astrophys. J.* **598**, 102 (2003) [arXiv:astro-ph/0309368].
- [4] A. G. Riess *et al.* [Supernova Search Team Collaboration], *Astrophys. J.* **607**, 665 (2004) [arXiv:astro-ph/0402512].
- [5] P. Astier *et al.*, [arXiv:astro-ph/0510447].
- [6] D. N. Spergel *et al.* [WMAP Collaboration], *Astrophys. J. Suppl.* **148**, 175 (2003) [arXiv:astro-ph/0302209].
- [7] D. N. Spergel *et al.* [WMAP Collaboration], arXiv:astro-ph/0603449.
- [8] M. Tegmark *et al.* [SDSS Collaboration], *Astrophys. J.* **606** (2004) 702 [arXiv:astro-ph/0310725].
- [9] S. Cole *et al.* [The 2dFGRS Collaboration], *Mon. Not. Roy. Astron. Soc.* **362**, 505 (2005) [arXiv:astro-ph/0501174].
- [10] For a recent review, see *e. g.* , W. J. Percival, arXiv:astro-ph/0508156.
- [11] O. Lahav, P. B. Lilje, J. R. Primack and M. J. Rees, *Mon. Not. Roy. Astron. Soc.* **251**, 128 (1991).
- [12] P. T. P. Viana and A. R. Liddle, *Mon. Not. Roy. Astron. Soc.* **281**, 323 (1996) [arXiv:astro-ph/9511007].
- [13] K. Coble, S. Dodelson and J. A. Frieman, *Phys. Rev. D* **55**, 1851 (1997).
- [14] L. Wang and P. Steinhardt, *Astrophys. J.* **508**, 483 (1998).
- [15] E. V. Linder and A. Jenkins, *Mon. Not. Roy. Astron. Soc.* **346**, 573 (2003) [arXiv:astro-ph/0305286].
- [16] See also, *e. g.* , R. Mainini, A. V. Macciò and S. A. Bonometto, *New Ast.* **8**, 173 (2003) [arXiv:astro-ph/0207581].
- [17] D. F. Mota and C. van de Bruck, *Astron. Astrophys.* **421**, 71 (2004) [arXiv:astro-ph/0401504].
- [18] S. A. Bidgoli, M. S. Movahed and S. Rahvar, [arXiv:astro-ph/0508323].
- [19] C. Horellou and J. Berge, *Mon. Not. Roy. Astron. Soc.* **360**, 1393 (2005) [arXiv:astro-ph/0504465].
- [20] N. J. Nunes, A. C. da Silva & N. Aghanim, arXiv:astro-ph/0506043.
- [21] M. Le Delliou, *JCAP* **0601**, 021 (2006) [arXiv:astro-ph/0506200].
- [22] J. E. Gunn and J. R. Gott, *Astrophys. J.* **176**, 1 (1972).
- [23] W. Press and P. Schechter, *Astrophys. J.* **187**, 425 (1974).
- [24] D. Huterer and M. S. Turner, *Phys. Rev. D* **64**, 123527 (2001) [arXiv:astro-ph/0012510].
- [25] H. K. Jassal, J. S. Bagla and T. Padmanabhan, *Mon. Not. Roy. Astron. Soc.* **356**, L11 (2005) [arXiv:astro-ph/0404378].
- [26] M. Chevallier and D. Polarski, *Int. J. Mod. Phys. D* **10**, 213 (2001) [arXiv:gr-qc/0009008].
- [27] J. Weller and A. Albrecht, *Phys. Rev. D* **65**, 103512 (2002) [arXiv:astro-ph/0106079].
- [28] R. Lazkoz, S. Nesseris and L. Perivolaropoulos, *JCAP* **0511**, 010 (2005) [arXiv:astro-ph/0503230].
- [29] U. Alam, V. Sahni, T. D. Saini and A. A. Starobinsky, *Mon. Not. Roy. Astron. Soc.* **344**, 1057 (2003) [arXiv:astro-ph/0303009].
- [30] U. Alam, V. Sahni and A. A. Starobinsky, *JCAP* **0406**, 008 (2004) [arXiv:astro-ph/0403687].
- [31] H. K. Jassal, J. S. Bagla and T. Padmanabhan, [arXiv:astro-ph/0601389].
- [32] C. Wetterich, *Phys. Lett. B* **594**, 17 (2004) [arXiv:astro-ph/0403289].
- [33] D. A. Dicus and W. W. Repko, *Phys. Rev. D* **70**, 083527 (2004) [arXiv:astro-ph/0407094].
- [34] C. P. Ma, R. R. Caldwell, P. Bode and L. M. Wang, *Astrophys. J.* **521**, L1 (1999) [arXiv:astro-ph/9906174].
- [35] C. Lacey and S. Cole, *Mon. Not. Roy. Astron. Soc.* **271**, 676 (1994) [arXiv:astro-ph/9402069].
- [36] A. Jenkins *et al.*, *Mon. Not. Roy. Astron. Soc.* **321**, 372 (2001) [arXiv:astro-ph/0005260].
- [37] See also, *e. g.* , N. J. Nunes and D. F. Mota, arXiv:astro-ph/0409481.
- [38] T. Padmanabhan, 1993, *Structure Formation in The Universe*, (Princeton University Press, Princeton)
- [39] P. J. E. Peebles, 1980, *The Large Scale Structure of the Universe*, Princeton University Press.

- [40] M. Davis, G. Efstathiou, C. S. Frenk and S. D. M. White, *Astrophys. J.* **292**, 371 (1985).
- [41] G. Efstathiou, C. S. Frenk, S. D. M. White and M. Davis, *Mon. Not. Roy. Astron. Soc.* **235**, 715 (1988).
- [42] W. Hu and R. Scranton, *Phys. Rev. D* **70**, 123002 (2004) [arXiv:astro-ph/0408456].
- [43] A. Jenkins *et al.*, *Mon. Not. Roy. Astron. Soc.* **321**, 372 (2001) [arXiv:astro-ph/0005260].
- [44] V. B. Johri, [arXiv:astro-ph/0409161].
- [45] T. Padmanabhan and T. R. Choudhury, *Mon. Not. Roy. Astron. Soc.* **344**, 823 (2003) [arXiv:astro-ph/0212573].
- [46] M. Tegmark *et al.* [SDSS Collaboration], *Phys. Rev. D* **69**, 103501 (2004) [arXiv:astro-ph/0310723].
- [47] See, *e.g.*, J. E. Carlstrom, G. P. Holder and E. D. Reese, *Ann. Rev. Astron. Astrophys.* **40**, 643 (2002) and also the site <http://spt.uchicago.edu>.